JACS
JOURNAL OF THE AMERICAN CHEMICAL SOCIETY
Article
pubs.acs.org/JACS

Microsecond Folding and Domain Motions of a Spider Silk Protein Structural Switch

Julia Ries,[†] Simone Schwarze,[†] Christopher M. Johnson,[‡] and Hannes Neuweiler*[,†]

[†]Department of Biotechnology & Biophysics, Julius-Maximilians-University Würzburg, Am Hubland, 97074 Würzburg, Germany
[‡]Medical Research Council Laboratory of Molecular Biology, Francis Crick Avenue, Cambridge CB2 0QH, United Kingdom

Supporting Information

ABSTRACT: Web spiders rapidly assemble protein monomers, so-called spidroins, into extraordinarily tough silk fibers. The process involves the pH-triggered self-association of the spidroin N-terminal domain (NTD), which contains a structural switch connecting spidroins to supermolecules. Single-molecule spectroscopy can detect conformational heterogeneity that is hidden to conventional methods, but motions of the NTD are beyond the resolution limit. Here, we engineered probes for 1 nm conformational changes based on the phenomenon of fluorescence quenching by photoinduced electron transfer into the isolated NTD of a spidroin from the nursery web spider *Euprosthenops australis*. Correlation analysis of single-molecule fluorescence fluctuations uncovered site-dependent nanosecond-to-microsecond movement of secondary and tertiary structure. Kinetic amplitudes were most pronounced for helices that are part of the association interface and where structural studies show large displacements between monomeric and dimeric conformations. A single tryptophan at the center of the five-helix bundle toggled conformations in ~100 μs and in a pH-dependent manner. Equilibrium denaturation and temperature-jump relaxation experiments revealed cooperative and ultrafast folding in only 60 μs. We deduced a free-energy surface that exhibits native-state ruggedness with apparently similar barrier heights to folding and native motions. Observed equilibrium dynamics within the domain suggest a conformational selection mechanism in the rapid association of spidroins through their NTDs during silk synthesis by web spiders.

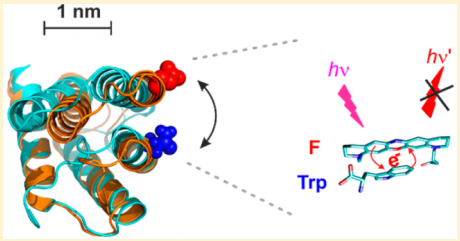

INTRODUCTION

Web-weaving spiders transform soluble fibroins, so-called spidroins, into solid silk fibers of extraordinary mechanical properties. Up to seven glands in the spider's abdomen are used to synthesize threads of properties tailored for their various tasks including prey capture, reproduction and shelter.[1] At the beginning of the process, spidroins are stored in soluble form in the ampulla of the spinning gland. On demand, they are assembled into fibers using carefully controlled chemical and mechanical stimuli during passage through a narrowing spinning duct.[1,2] Stimuli include changes in salt composition, pH and shear forces along the duct. Focus in the field of material sciences is on the man-made reproduction of spider silk,[2,3] but the molecular mechanisms of the underlying protein association events are only understood in parts. The bulk of a spidroin sequence consists of repetitive peptide motifs of simple amino acid composition that form mainly β-sheet structure in fibers. The large, repetitive sequence elements are flanked by the globular terminal domains. The N-terminal domain (NTD) is the most conserved sequence part of a spidroin and similar in different spider species and types of glands, suggesting a pivotal role in the production of silk.[4] Spidroins from the major ampullate gland form tough dragline silk that is used as thread for the web-frame or lifeline. The NTD of spidroin 1 from the major ampullate gland of the nursery web spider *Euprosthenops australis* is a 14-kDa five-helix bundle.[5] It contains a pH-sensitive relay that controls self-association through a sophisticated mechanism. A change of solution pH from 7 to 6 in the distal part of the spinning duct causes the NTD to self-associate thereby connecting spidroins to supermolecules in silk fibers.[6−8] Extensive mutagenesis in combination with various biophysical techniques shows that specific amino acid side chain charges on the protein surface are involved in the process.[5,9,10]

Structural studies have identified differences in monomeric and dimeric conformations of the NTD.[11] In the monomer, helices that form the dimerization interface are rearranged such that self-association is sterically excluded. In the dimer, instead, helices form a perfectly complementary self-association interface. Rearrangements appear to be driven by a single tryptophan (Trp) that wedges in the center of the five-helix bundle.[11] The different structural forms have been observed by solution-NMR spectroscopy and crystallography showing that they are not the result of crystal constraints.[12] Pictures from structural studies, however, are static. The observation of conformational motions that underlie the structural switch in solution is hampered by their local nature. Further, equilibrium conformational changes are often masked in the average signal of the vast ensemble of molecules probed using conventional spectroscopy. Single-molecule spectroscopy, on the other hand, can detect the heterogeneous nature of protein conformation.

Received: September 1, 2014
Published: November 10, 2014

   dx.doi.org/10.1021/ja508760a | J. Am. Chem. Soc. 2014, 136, 17136−17144

Its combination with fluorescence resonance energy transfer (smFRET) between a donor and an acceptor fluorophore is widely applied in the study of biomolecular interaction, conformation, and dynamics.[13−16] The smFRET signal is typically most sensitive where the distance between donor and acceptor labels is between 2 and 8 nm.[17] But displacement of helices in the NTD is on a scale of only ∼1 nm. Contact-induced quenching of organic fluorophores by the amino acid Trp through photoinduced electron transfer (PET),[18] on the other hand, is a short-range tool for detecting protein conformation and complementary to FRET.[17,18] The combination of PET with correlation analysis of single-molecule fluorescence fluctuations (PET-FCS) establishes a nanosecond spectroscopic tool for studying protein dynamics at the 1 nm scale.[19,20]

Here, we engineered PET reporters into the isolated NTD of spidroin 1 from the major ampullate gland of *E. australis* to explore conformational motions underlying the structural switch. PET-FCS shows that the NTD is a highly dynamic protein. Helices that have previously been identified to rearrange upon association are actually mobile and dynamic on a microsecond time scale already in the monomer. The single Trp located at the center of the helix-bundle toggles conformation on a 100-μs time scale and in a pH-dependent manner. Temperature-jump (T-jump) Trp fluorescence experiments showed ultrafast and cooperative folding in only 60 μs. Observed equilibrium dynamics of the NTD monomer suggest a conformational selection mechanism in the early stage of rapid association of spidroins through their NTDs in the spinning duct of web spiders.

RESULTS

Design of Fluorescence Probes for NTD Motions. Organic fluorophores form $\pi-\pi$ stacking interactions with the side chain of Trp at distances ≤1 nm. Electronic overlap at van der Waals contact facilitates efficient fluorescence quenching by PET from Trp to the fluorophore in the electronically excited state.[21] We engineered fluorophore and Trp pairwise as PET reporters into the NTD at solvent-exposed sites. Sites were chosen such that fluorophore and Trp were located at 1 nm distance with respect to each other facilitating fluorescence quenching. Monomer and dimer conformations of the NTD and the reporter design are shown in Figure 1. Trp (W) and cysteine (Cys, C) residues were introduced individually by site-directed mutagenesis. Cys side chains of synthesized protein material were modified chemically using a thiol-reactive derivative of the oxazine fluorophore AttoOxa11. Three constructs were generated to probe motions of helices with respect to each other. Q50C−N21W probed helix-1/helix-2 (*H1*/*H2*), S51C-A68W probed helix-2/helix-3 (*H2*/*H3*), and S99C-Q122W probed helix-4/helix-5 (*H4*/*H5*). We aimed at measuring motions of native Trp W10 that changes tertiary structure in monomer and dimer conformations by involving it in a PET reporter: mutant G3C at the N-terminus places AttoOxa11 in close structural vicinity to W10 (Figure 1A and 1B). The C-terminal turn segment of *H3* surrounding residue S83 undergoes a coil-to-helix transition upon dimerization.[11] We targeted this segment by PET reporter G88C−S83W (Figure 1D). Thus, a total of five different constructs were generated to probe motions at five different sites spanning the entire structure of the NTD.

PET reporters were engineered on the background of a pseudowild-type protein[11] where alanine at position 72 of helix-3, which is at solvent-exposed site on the association interface, was replaced by an arginine (A72R). The bulky arginine side chain prevents dimerization by local effects while maintaining the structural integrity of the NTD; the folds of mutant and wild-type protein are identical.[11] We used pseudowild-type A72R to avoid complications in data interpretation caused by potential changes in molecularity during experiments carried out under solution conditions that favor dimerization. In the following, we denote the presence of mutation A72R in NTD constructs by an asterisk (*). Self-association of the NTD can be probed by intrinsic Trp fluorescence. W10 is buried in the monomer conformation but takes a surface position in the dimer.[11] As a consequence, fluorescence of W10 is quenched by solvent water molecules upon dimerization[5,7] (Supporting Information Figure S1A). Trp fluorescence spectra of NTD*, instead, exhibit no significant changes between pH 7.0 and 6.0 showing that the pseudowild-type protein does not dimerize (Supporting Information Figure S1B), in agreement with previous results.[11]

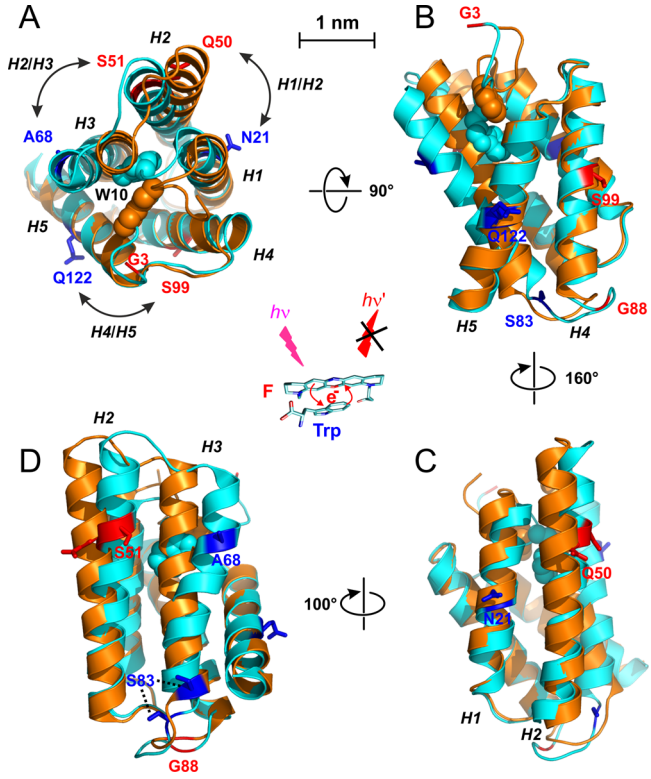

Figure 1. Design of PET reporters for NTD conformational motions. Superposition of monomeric (cyan) and dimeric (orange) conformations of the NTD (PDB IDs 2LPJ and 3LR2)[11] in cartoon representation. Helices *H1* to *H5* are indicated. The second subunit of structure 3LR2 is omitted for reasons of clarity. Panels (A−D) show different domain orientations. A 1 nm scale bar is indicated. Amino acids that were mutated to Trp and Cys in pairwise combinations for subsequent fluorescence modification to generate PET reporters are highlighted (blue and red stick representations, respectively). The side chain of native Trp W10 is shown in sphere representation. Fluorophore (F) and Trp in $\pi-\pi$ stacking interaction geometry[21] quenching fluorescence by PET are depicted at the center of the figure.

Kinetics of NTD Conformational Motions Probed by PET-FCS. Fluorescence correlation spectroscopy (FCS) analyzes fluorescence fluctuations of molecules diffusing stochastically through the detection volume of a confocal microscope setup by Brownian motion.[22] Fluorescence

dx.doi.org/10.1021/ja508760a | J. Am. Chem. Soc. 2014, 136, 17136−17144

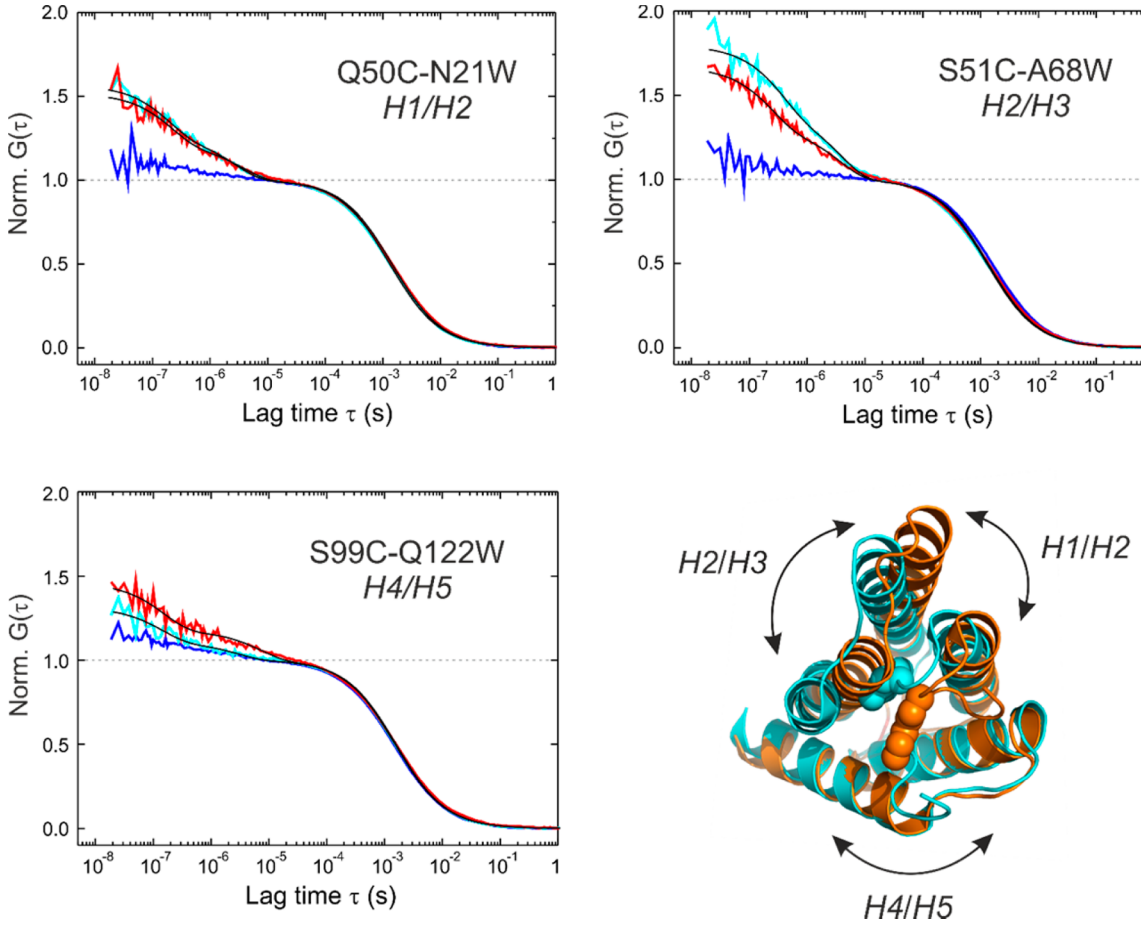

Figure 2. PET-FCS of helix motions. ACFs recorded from NTD* constructs reporting on helix motions. Data recorded at pH 7.0 (monomer conditions) and pH 6.0 (dimer conditions) are colored cyan and red, respectively. ACFs of control samples lacking the engineered Trp side chain are colored blue. ACFs were normalized to *N*, the average number of molecules in the detection focus, for reasons of clarity. Broken horizontal lines indicate the amplitudes of decays that result from translational diffusion. Relaxations resulting from conformational fluctuations emerge on top of the diffusion decays. Black solid lines are data fits using a model for a diffusing globule with two single-exponential relaxations. Pairs of helices probed by individual reporters are indicated in the structural alignment of monomeric (cyan) and dimeric (orange) NTD (PDB IDs 2LPJ and 3LR2).

fluctuations are analyzed by calculating the second-order autocorrelation function (ACF) of fluorescence intensity time traces. Any process that gives rise to a fluctuation of fluorescence emission results in a decay of the ACF at a characteristic time constant. In PET-FCS, fluorescence quenching by PET transforms protein conformational fluctuations into fluorescence fluctuations that emerge as additional decay(s) in the ACF on top of the one originating from molecular diffusion.[20]

We recorded ACFs of PET reporter-containing NTD* both at pH 7.0 and pH 6.0, i.e., under solution conditions that favor the monomeric and dimeric form, respectively. Figure 2 shows ACFs recorded from the constructs with the reporters located on helices. Constructs probing motions of native W10 and a disordered loop segment connecting H3 and H4 are shown in Figure 3. All ACFs exhibited decays at a lag time of ∼1.5 ms that arose from translational diffusion of NTD molecules through the detection focus. PET reporters caused additional decays on top of the ones originating from diffusion. ACFs fitted well to an analytical model for diffusion of a globule containing two additional exponential relaxations on the nanosecond-to-microsecond (ns-μs) time scale. To asses if these additional decays truly arose from PET, we synthesized and measured a control sample for each of the constructs, which lacked the engineered Trp (blue data). For N-terminal construct G3C* probing motions of native W10 we designed a control that had AttoOxa11 labeled to the C-terminus (mutant A137C*). In all of these controls, the additional decays were virtually absent showing that those observed in the presence of Trp resulted from PET quenching. Residual fluctuations observed for some of the control samples can be explained by the fact the AttoOxa11 is an environmentally sensitive fluorophore that translates structural fluctuations associated with changes in polarity of its microenvironment into minor modulations of fluorescence intensity. Kinetics of PET reporter-containing constructs were not intrinsic to the PET reaction because electron transfer between Trp and fluorophore is on the very fast femtosecond-to-picosecond time scale.[23] Further, the applied oxazine fluorophore is void of photophysical fluctuations like populated triplet states under the applied experimental conditions.[18] To rule out with certainty the possible presence of photophysical fluctuations, we recorded ACFs of representative constructs at various excitation power (Supporting Information Figure S2). The observed fluctuations were independent of excitation power and had thus no photophysical origin. We concluded that the ns-μs decays in PET-FCS data of the NTD reported on conformational motions.

dx.doi.org/10.1021/ja508760a | J. Am. Chem. Soc. 2014, 136, 17136−17144

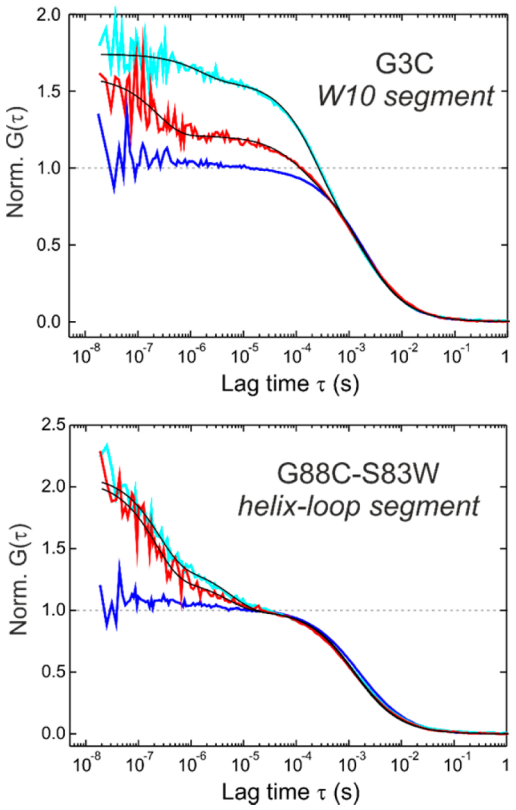

Figure 3. PET-FCS of Trp-wedge and loop segment. ACFs recorded from NTD* constructs reporting on motion of W10 and the disordered loop segment connecting *H3* and *H4*. Data recorded at pH 7.0 (monomer conditions) and pH 6.0 (dimer conditions) are colored cyan and red, respectively. ACFs of control samples lacking the engineered Trp side chain are colored blue. Construct G3C* that probes motion of native W10 at the N-terminus had fluorescently modified mutant A137C* at the C-terminus as a control. ACFs were normalized to *N*, the average number of molecules in the detection focus, for reasons of clarity. Broken horizontal lines indicate the amplitudes of decays that result from translational diffusion. Black solid lines are data fits using a model for a diffusing globule with two single-exponential relaxations.

The PET decays in ACFs varied with reporter position. For probes reporting on motions of helices, namely, Q50C−N21W*, S51C-A68W*, and S99C-Q122W*, the highest amplitude of μs motion was observed for helix-pair *H2*/*H3* (S51C-A68W*) followed by *H1*/*H2* (Q50C−N21W*). *H4*/*H5* (S99C-Q122W*) had kinetic amplitudes hardly above that of the control sample. The rank order of observed decay amplitudes followed the magnitude of helix displacements seen between monomeric and dimeric NTD conformations (Figure 2). PET-FCS kinetic parameters are summarized in Table 1. Time constants of helix motions were on a similar 3-μs scale and changed little with pH. There was an additional, faster kinetic phase at ∼200 ns. This 200 ns phase did not originate from the flexibility of linkers connecting the aromatic moieties of fluorophore and Trp to the protein backbone: PET-FCS data of the reporter system placed on conformationally stiff polyproline peptides are kinetically silent.[24] Moreover, data of short, unstructured poly-GS-peptides show no contributions from flexible linkers,[25] which are likely to occur on a faster picosecond time scale. The observed 200 ns time constant compares with the time scale of helix−coil transitions in model peptides.[26] Kern et al.[16] assign ∼100 ns kinetics to tier-1 motions that reflect collective movement of short chain segments in proteins. Lange et al.[27] find from a combination of experiment and computer simulation evidence for collective protein motions on that time scale in native ubiquitin. Bourgeois et al.[28] detect, using time-resolved Laue diffraction experiments, a 100−300 ns relaxation in myoglobin and assign this relaxation to helix motions. It thus seems reasonable to assume that the 200 ns relaxation observed in our PET-FCS data reports on a rapid, local mode of helix motion.

PET amplitudes were pronounced in construct G3C* that was designed to probe motion of W10 (Figure 3). The main relaxation was on a slower 100-μs time scale but clearly distinct from the 1.5 ms decay that resulted from diffusion (Supporting Information Figure S3). There was a change of kinetics at this site with pH (Figure 3; Table 1). The time constant (amplitude) at pH 7.0 was 230 ± 10 μs (0.57 ± 0.01) and decreased to 100 ± 20 μs (0.20 ± 0.02) at pH 6.0. At pH 7.0, there was an additional ∼2-μs phase of marginal amplitude which turned into a 250 ns relaxation of significant amplitude at pH 6.0. Construct G88C−S83W*, which was designed to probe the loop segment connecting *H3* and *H4*, had a ∼150 ns relaxation of substantial amplitude, as expected for a disordered segment undergoing loop closure,[19] which changed little with pH. There was an additional 3−4-μs relaxation of smaller amplitude. We note that a microscopic analysis of native-state kinetics was precluded by the fact that the brightness of interconverting conformational states was unknown.[20]

To assess whether mutation A72R influenced the measured motions, we recorded ACFs of constructs with PET reporters engineered on the background of wild-type NTD. The wild-type protein should be largely monomeric at low sample

Table 1. Kinetics of Native-State Motions of NTD*

Construct	pH	$a_1{}^a$	$\tau_1{}^a$ (μs)	$a_2{}^a$	$\tau_2{}^a$ (μs)
Q50C−N21W*	7.0	0.26 ± 0.03	2.8 ± 0.4	0.30 ± 0.01	0.20 ± 0.06
	6.0	0.24 ± 0.02	3.0 ± 0.6	0.36 ± 0.08	0.15 ± 0.07
S51C-A68W*	7.0	0.43 ± 0.03	3.5 ± 0.3	0.39 ± 0.04	0.29 ± 0.06
	6.0	0.35 ± 0.04	3.1 ± 0.5	0.36 ± 0.01	0.16 ± 0.07
S99C-Q122W*	7.0	0.12 ± 0.03	2.7 ± 0.8	0.19 ± 0.01	0.15 ± 0.09
	6.0	0.18 ± 0.02	6 ± 2	0.28 ± 0.01	0.13 ± 0.05
G3C*	7.0	0.57 ± 0.01	230 ± 10	0.17 ± 0.03	1.9 ± 0.9
	6.0	0.20 ± 0.02	100 ± 20	0.41 ± 0.07	0.20 ± 0.02
G88C−S83W*	7.0	0.39 ± 0.06	4 ± 1	0.81 ± 0.06	0.18 ± 0.06
	6.0	0.4 ± 0.1	3 ± 2	1.0 ± 0.2	0.13 ± 0.08

[a] a_1/a_2 and τ_1/τ_2 are the relaxation amplitudes and corresponding time constants. Errors are standard deviations of three measurements.

dx.doi.org/10.1021/ja508760a | J. Am. Chem. Soc. 2014, 136, 17136−17144

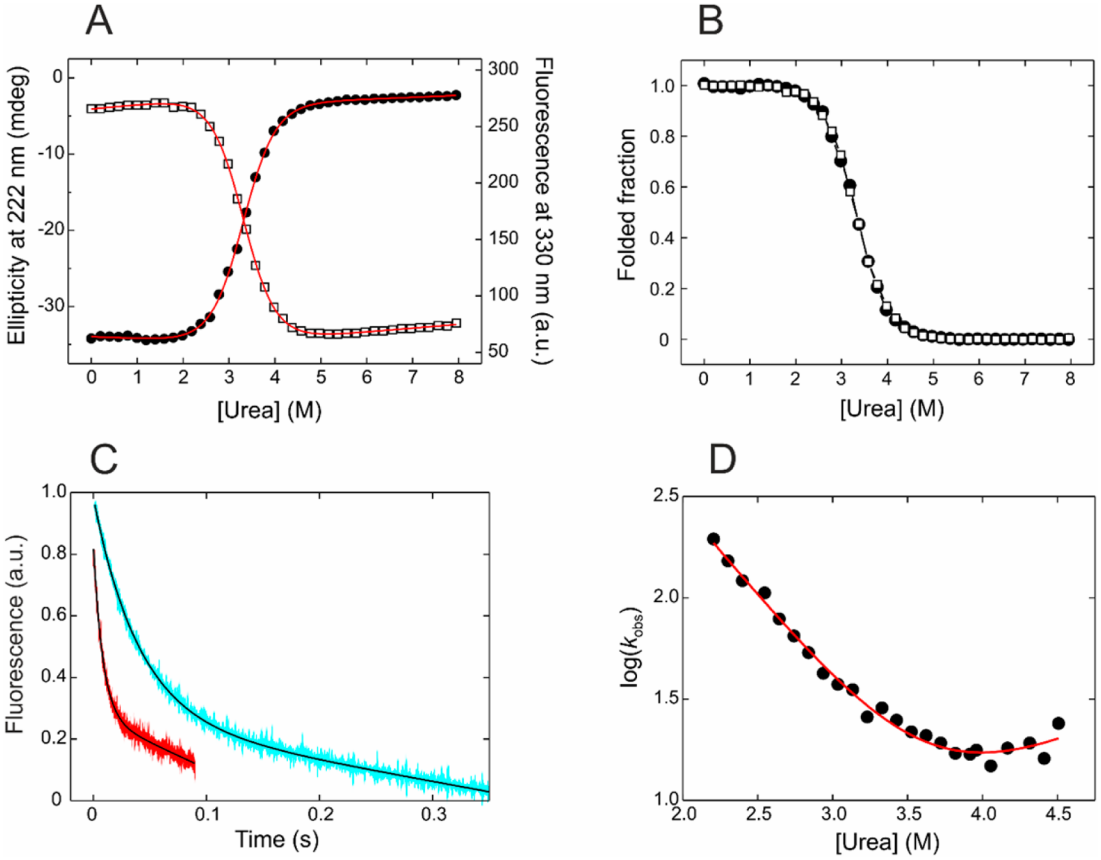

Figure 4. Equilibrium denaturation and folding kinetics. (A) Equilibrium chemical denaturation of wild-type NTD at pH 7.0 probed by far-UV CD spectroscopy (closed circles) and by Trp fluorescence (open squares). Red lines are data fits using the thermodynamic model for a two-state equilibrium. (B) Far-UV CD (closed circles) and Trp fluorescence (open squares) data normalized to the fraction of folded protein. (C) Kinetic transients of NTD folding measured by T-jump Trp fluorescence spectroscopy. Representative relaxations measured at 2.5 M urea (red data) and at 3.5 M urea (cyan data) are shown. Black lines are fits to the data using a single-exponential decay function containing a linear baseline drift. (D) Observed relaxation rate constants plotted versus urea concentration (chevron plot). The red line is a fit using the kinetic model for a barrier-limited two-state transition.

Table 2. Thermodynamic and Kinetic Parameters of NTD Folding[a]

	$[\text{urea}]_{50\%}$ (M)	m_{D-N} (kcal mol^{-1} M^{-1})	ΔG_{D-N} (kcal/mol)	k_f (s^{-1})	k_u (s^{-1})	m_f (kcal mol^{-1} M^{-1})	m_u (kcal mol^{-1} M^{-1})
Fluorescence	3.31 ± 0.01	1.69 ± 0.02	5.60 ± 0.07	16 900 ± 5900	0.6 ± 0.5	1.22 ± 0.08	0.45 ± 0.14
CD	3.30 ± 0.01	1.69 ± 0.03	5.60 ± 0.10	–	–	–	–

[a]Errors are standard errors from data fits. $[\text{urea}]_{50\%}$ denotes the transition midpoint.

concentrations applied in PET-FCS. For these control experiments we selected constructs that exhibited pronounced ACF decays, namely, Q50C−N21W, S51C-A68W, G3C, and G88C−S83W. Wild-type ACFs together with data analysis are provided as Supporting Information (Figure S4 and Table S1). The pattern of PET decays was conserved for all wild-type constructs, showing similar amplitudes and time constants compared with kinetics obtained for mutant A72R. Minor differences in kinetic quantities can be explained by the fact that wild-type NTD is prone to form bimolecular interactions in contrast to mutant A72R.

Folding of the NTD. To explore the conformational free-energy surface of the NTD beyond the native basin we characterized folding equilibrium and kinetics using circular dichroism (CD) and Trp fluorescence experiments. We used wild-type protein for these experiments. The far-UV CD signal at 222 nm reports on helical secondary structure whereas Trp fluorescence measures the tertiary environment of W10. Urea denaturation was performed in pH 7.0 buffer where the domain is monomeric. Unfolding was signaled by a decrease of Trp fluorescence caused by solvent-exposure of the indole side chain, similar to the process of self-association where W10 moves from buried to solvent-exposed position (Supporting Information Figure S5). We measured equilibrium unfolding by monitoring both far-UV CD and Trp fluorescence signals (Figure 4A). The data sets fitted well to a model for a two-state equilibrium between native (N) and denatured (D) states. Denaturation curves, normalized to the fraction of folded protein, superimposed very well (Figure 4B). The transition midpoint, $[\text{D}]_{50\%}$, the equilibrium m-value, m_{D-N}, and the standard free energy of folding, ΔG_{D-N}, obtained from fluorescence and CD signals were in excellent agreement consistent with cooperative two-state folding (Table 2).

Kinetics of folding was measured using resistive-heating T-jump Trp fluorescence spectroscopy. Fluorescence transients were obtained from 3-K jumps in the unfolding transition region between 2.2 and 4.5 M urea. Representative transients together with data fits are shown in Figure 4C. All transients

dx.doi.org/10.1021/ja508760a | J. Am. Chem. Soc. 2014, 136, 17136−17144

fitted well to a single-exponential decay function that contained a linear baseline drift. The linear drift originated from Trp photobleaching, which was evident from inspection of the pre- and postrelaxation regions of T-jump data (Supporting Information Figure S6A and S6B). Fluorescence intensities observed in the prerelaxation time traces, i.e., the fluorescence intensities before the actual T-jump, exhibited the same linear drift as observed in the postrelaxation baselines. The linear drift was further observed for a fully denatured protein sample (Supporting Information Figure S6C). We analyzed folding relaxations by plotting the observed rate constants (k_{obs}) extracted from exponential data fits versus urea concentration and fitting a model of a barrier-limited two-state transition (Figure 4D). The typical chevron-shape of this plot appeared tilted because the kinetic *m*-value of folding, m_f, was significantly larger than that of unfolding, m_u. As a consequence, the unfolding limb of the chevron was poorly defined and lead to a comparatively large error in the extrapolated rate constant of unfolding. The obtained kinetic parameters of folding are summarized in Table 2. The folding time constant of the NTD in the absence of urea was on the microsecond scale. As expected for two-state folding,[29] equilibrium and kinetic quantities were in good agreement. The equilibrium *m*-value, $m_{eq} = 1.69 \pm 0.03$ kcal mol^{-1} M^{-1}, matched the sum of kinetic folding and unfolding *m*-values, $m_{kin} = m_f + m_u = 1.7 \pm 0.2$ kcal mol^{-1} M^{-1}. The standard free energy of folding obtained from equilibrium denaturation, $\Delta G_{D-N} = 5.7 \pm 0.1$ kcal mol^{-1}, was in good agreement with the value of $\Delta G_{D-N} = 6.0 \pm 0.7$ kcal mol^{-1} obtained from extrapolated rate constants of folding and unfolding ($\Delta G_{D-N} = -RT \ln(k_f/k_u)$). The high Tanford β-value, $\beta_T = m_f/(m_f + m_u) = 0.7 \pm 0.1$, indicated that the NTD folds through a compact and native-like transition state.

DISCUSSION

Mechanism and structural changes facilitating self-association of the spidroin NTD in the spinning duct of web spiders are only understood in parts. Recently, Kronqvist et al.[12] proposed from site-directed mutagenesis in combination with pH-dependent, chemical denaturation experiments a multistep process of self-assembly that involves sequential protonation of specific amino acid side chains as the solution-pH drops along the spinning duct. Similarly, computer simulations by Wallace et al.[30] predict that the initial assembly of the monomers is followed by protonation of specific side chains, leading to release of water molecules from the association interface stabilizing the dimer. Very recently, Andersson et al.[31] measured, using micro-electrodes, the solution pH at various positions along a spinning duct and found that it dropped to pH 5.5, possibly even below in the very distal part close to the exit spigot. A scenario where initial association at pH 6 is followed by further protonation events downstream the spinning duct to consolidate the assembly seems possible.

In light of these proposals, the present work concerns the early events of pH-triggered self-association in the spinning duct. Structural studies[11] show that the NTD monomer is a more expanded five-helix bundle compared with the dimer. Helix-3 is tilted out of the dimerization interface leading to a fold that is incompatible of self-association. Displacement of helices appears to be driven by Trp W10 that wedges itself into central position in the monomer conformation.[11] Since dimerization is triggered by a change of pH, one may speculate that protonation drives conformational rearrangements that form the association interface. But structures determined at pH 7 and pH 6 of mutant A72R that traps the NTD in the monomeric state superimpose,[11] with no detectable changes of Trp fluorescence emission (Supporting Information Figure S1B). However, structural studies commonly resolve the highest populated conformation biased to a free energy minimum and a fold thus appears static. Many proteins move in order to function and access transiently populated states of higher free energy that are difficult to detect experimentally.[16] Energy landscape theory accounts for this conformational heterogeneity described as substates on a rugged energy landscape.[32,33] While the heterogeneous and dynamic nature of protein conformation remains invisible to conventional spectroscopy, advanced NMR methods and single-molecule spectroscopy can detect such "excited" protein states.[14,16,34] In the present study, we combined PET with single-molecule fluorescence fluctuation analysis and revealed equilibrium conformational dynamics of the NTD. As single-molecule method PET-FCS is capable of detecting low-populated conformational states as dynamic heterogeneity of molecules stochastically diffusing through the confocal detection volume. We observed ~3-μs relaxations of helices with amplitudes that were largest for *H2*/*H3* and *H1*/*H2*, which form the association interface. The time scale of motion compares with the ~10-μs relaxation detected for a loose helix in a protein folding intermediate.[35] *H4*/*H5*, on the other hand, had marginal amplitudes that were hardly above those of the control sample (Figure 2). The rank order of PET-FCS amplitudes follows the magnitude of helix displacements seen between the monomer and dimer conformations. Structural studies show that, on dimerization, helices *H3* and *H2* move from their displaced orientation back into the domain while *H4* and *H5*, which are located outside the association interface, remain fairly static.[11] Helix movement is accompanied by relocation of W10 from buried to solvent-exposed position. The present results show that these W10 movements occur rapidly and at equilibrium already in the monomer, both at pH 7 and at pH 6. Amplitude and time constant of W10 motion changed significantly with pH. It thus appears that the conformational ensemble undergoes a pH-induced shift before association, which may involve population of association-competent conformations at pH 6. The additional nanosecond kinetic phase that emerged in construct G3C* at pH 6.0 (Figure 3; Table 1) likely reports on rapid loop closure of the solvent-exposed W10-segment. Loop closure kinetics of unfolded chains occur on the ~100 ns time scale[19,36] and also emerged as main decay in construct G88C–S83W* that probed the disordered loop connecting *H3* and *H4*.

The observed equilibrium dynamics can be understood as native-state ruggedness on the free-energy surface of the NTD (Figure 5A). Since the dynamics were detected for structural elements that move on association, the finding suggests a "conformational selection" mechanism in the early phase of pH-triggered self-association (Figure 5B). "Conformational selection" is a modern model of molecular recognition and distinct from the traditional "induced fit" mechanism.[37] "Induced fit" assumes that a protein in solution populates only a single conformation and that a change of conformation on binding is induced by the association event. "Conformational selection", on the other hand, assumes that a protein populates many conformations in dynamic equilibrium even in the absence of the binding partner. The partner then selects from this ensemble of conformations the one that exhibits the complementary association interface. Boehr et al.[37] point out

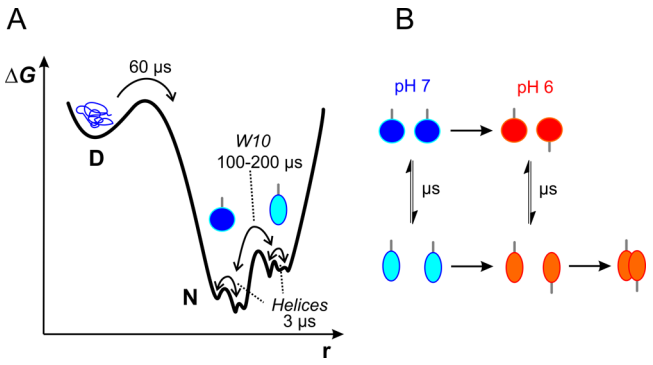

Figure 5. Free energy profile of the NTD and proposed mechanism of self-association. (A) Schematic cross section through the conformational free energy surface deduced from kinetics of folding and native-state motions. ΔG is plotted versus an arbitrary reaction coordinate *r*. Denatured (D) and native (N) state basins are separated by an energy barrier that gives rise to cooperative folding. The native basin is rugged and exhibits energy barriers to motions of helices and Trp W10 that toggles conformations at the center of the helix bundle. Spheres and ovals represent two different native conformations in dynamic equilibrium. Gray sticks indicate the positions where the repetitive spidroin sequence segments append. (B) Scheme of pH-triggered self-association via "conformational selection". The observed μs equilibrium dynamics suggest that the monomeric form transiently populates association-competent conformations (orange ovals) that are subsequently selected by the complementary binding interface.

that both mechanisms are not exclusive and may act together: initial binding by "conformational selection" can be followed by "induced fit" consolidating structural changes within the bound state. The coupling of "conformational selection" and "induced fit" emerges as a likely scenario in NTD self-assembly, in light of sequential protonation events beyond pH 6.0 proposed by Kronqvist et al.[12]

The spidroin NTD investigated here originates from a major ampullate gland that is being used by web spiders to synthesize dragline silk for building the web frame or a lifeline.[1] Evolutionary pressure is on the speed of dragline synthesis: during roping or a vertical fall, silk threads are being extruded at ~1 m/s and sometimes even faster.[1,38,39] At such high reeling speed, the residence time of spidroins in the acidified NTD assembly zone of the spinning duct may be only ~1 ms. Stopped-flow experiments show that self-association of the isolated NTD at pH 6 has a rate constant of 3×10^8 M^{-1} s^{-1}, which is 3 orders of magnitude faster than the basal rate constant of protein−protein association and close to the diffusion speed limit.[10] Spidroin concentrations in spinning glands are on the order of 1 mM^1 and this concentration, together with the above rate constant, translates into an association time of ~3 μs. The association time in a spinning gland, however, will be slower. The terminal domains take only ~5% of the ~300 kDa spidroin sequence and diffusional mobility of NTDs will be slaved by slow motion of the large repetitive sequence. Moreover, the high spidroin concentration of ~50% (w/v) in a gland induces conditions of macromolecular crowding. The spinning dope is a viscid liquid crystalline showing non-Newtonian fluid dynamics[1] that will further slow diffusion of NTDs. The intramolecular μs dynamics observed here may thus be sufficiently fast to facilitate "conformational selection" in the early stage of self-association. The salt composition of the spinning dope changes along the duct.[40] Increased levels of solution ionic strength abolish NTD dimerization.[7,8] Stopped-flow experiments, however, show that the population shift toward the monomeric form at high ionic strength is a result of an increased rate constant of dissociation while the rate constant of association remains unaffected by salt.[10] The mechanism of NTD association thus appears unaffected by changes of ionic strength along the spinning duct.

We extended the exploration of the NTD free-energy surface beyond the native well by measuring kinetics of folding. Equilibrium denaturation experiments suggested that the domain is a cooperative two-state folder, which was confirmed by chevron analysis of folding kinetics. The high β_T-value (Table 2) indicated that the NTD folds through a late transition state, which is common for small single-domain proteins.[41,42] The extrapolated folding time constant of 60 ± 20 μs was remarkably fast and identified the spidroin NTD as a new member of the selected group of proteins that fold near the "speed limit".[26] Fast folding suggests that the denatured well of the free-energy surface is smooth and minimally frustrated. Domains that fold within μs are prime model systems to explore fundamental mechanisms of protein folding because the submillisecond time scale can be accessed by both experiment and computer simulation.[43] Synergistic approaches from both disciplines can provide atomic-detailed descriptions of folding pathways. In this regard, the spidroin NTD is a particularly interesting system because the fold is unique with no homologue identified so far. The sequence is very unusual with ~40% alanine/serine content and only 9% charged side chains. By contrast, the average content of charged side chains in proteins is 29%.[44] The observed similarity of time constants of NTD folding and toggling native-state motion of W10 indicates that both conformational events experience similar free-energy barrier heights (Figure 5A). Motion of W10 reflects a change of tertiary structure. It is tempting to speculate that formation of tertiary interactions may thus also be the rate-limiting step of NTD folding. Further studies are required to characterize the nature of energy barriers separating denatured and native basins, as well as the barriers separating native functional substates and their pH-dependence. This may finally complete our understanding of a remarkable molecular switch that nature evolved for the synthesis of silk fibers by web spiders.

MATERIALS AND METHODS

Protein Synthesis, Mutagenesis and Fluorescence Modification. The NTD from spidroin 1 of the major ampullate gland of the nursery web spider *E. australis* was overexpressed in *Escherichia coli* C41 (DE3) bacterial cells transformed with a modified pRSETA vector containing the NTD gene. The construct contained an N-terminal His_6-tag followed by the thrombin recognition sequence for proteolytic removal. Single-point mutants were generated using the QuikChange mutagenesis protocol (Stratagene). Overexpressed NTDs and mutants thereof were isolated from clarified cell lysate by Ni-NTA affinity chromatography followed by proteolytic cleavage of the His_6-tag using thrombin from bovine plasma (Sigma). The thrombin-digested eluate from Ni-NTA chromatography was concentrated using centrifugal concentrators (Sartorius Vivaspin, 5 kDa MWCO). The concentrated protein was purified to homogeneity using size exclusion chromatograpy (SEC) on a Superdex 75 column (GE Healthcare) equilibrated with 200 mM ammonium bicarbonate. The pooled fractions from SEC were lyophilized and stored at −20 °C. NTD mutants were modified with the thiol-reactive maleimide derivative of the oxazine fluorophore AttoOxa11 (Atto-Tec). Labeling was carried out using a 10-fold molar excess of fluorophore reacted for 2.5 h at 25 °C in 50 mM 3-(morpholino)propanesulfonic acid (MOPS) pH 7.5

dx.doi.org/10.1021/ja508760a | J. Am. Chem. Soc. 2014, 136, 17136−17144

containing 6 M guanidinium chloride and a 10-fold molar excess of *tris*(2-carboxyethyl)phosphine (TCEP; Sigma) to prevent thiol oxidation. Labeled protein was isolated from nonreacted dye using SEC.

PET-FCS Experiments. PET-FCS was performed on a custom-built confocal fluorescence microscope setup that consisted of an inverse microscope body (Zeiss Axiovert 100 TV) equipped with a diode laser emitting at 637 nm as excitation source (Coherent Cube). The laser beam was coupled into an oil-immersion objective lens (Zeiss Plan Apochromat, 63×, NA 1.4) via a dichroic beam splitter (Omega Optics 645DLRP). The average laser power was adjusted to 400 μW before entering the back aperture of the microscope using an optical density filter. The fluorescence signal was collected by the same objective, filtered by a band-pass filter (Omega Optics 675RDF50), and imaged onto the active area of two fiber-coupled avalanche photodiode detectors (APDs; PerkinElmer, SPCM-AQRH-15-FC) using a cubic nonpolarizing beam splitter (Linos) and multimode optical fibers of 100 μm diameter. The signals of the APDs were recorded in the cross-correlation mode using a digital hard-ware correlator device (ALV 5000/60 multiple tau digital real correlator) to bypass detector dead-time and after-pulsing effects. Fluorescently modified NTDs were diluted to 1 nM samples in aqueous buffered solutions containing 0.3 mg/mL bovine serum albumin (BSA) and 0.05% Tween-20 as additives to suppress glass surface interactions. Measurements were carried out in monomer and dimer solution conditions using 50 mM phosphate buffer pH 7.0 (with the ionic strength adjusted to 200 mM using potassium chloride) and 20 mM 2-(*N*-morpholino)ethanesulfonic acid (MES) buffer pH 6.0, respectively. Samples were filtered through a 0.2 μm syringe filter before measurement, transferred onto a microscope slide and covered by a coverslip. A 1-nM sample yielded an average of ∼20 molecules in the detection focus. Sample temperature was set to 25 °C using a custom-built objective heater. For each sample, three individual ACFs were recorded of 15 min measurement time each.

Steady-State Fluorescence and Far-UV CD Spectroscopy. Steady-state fluorescence emission spectra were acquired using a Jasco FP-6500 spectrofluorometer. Samples were measured at 10 μM protein concentration in a 10 mm path-length fluorescence cuvette. Far-UV CD spectroscopy was performed using a Jasco J-815 spectropolarimeter and a 1 mm path-length cuvette containing 10 μM protein. Chemical denaturation experiments were performed by manual titration between 0 and 8 M urea. Denaturation experiments were carried out under monomer solution conditions in 50 mM MOPS pH 7.0 with the ionic strength adjusted to 200 mM using potassium chloride. Trp was excited at 280 nm and fluorescence emission was recorded at 330 nm. The far-UV CD signal was recorded at 222 nm probing the NTD α-helix. Temperature of samples was controlled using a Peltier thermocouple set to 25 °C throughout all measurements.

T-Jump Spectroscopy. Folding relaxation kinetics was measured by Trp fluorescence spectroscopy using a resistive-heating T-jump machine (modified Hi-Tech PTJ-64 capacitor-discharge apparatus). T-jumps of 3 K were induced by rapid discharge of a 30 nF capacitor through a 5 × 5 mm optical cell resulting in an instrumental heating time of ∼20 μs. Sample concentration was 50 μM protein in 50 mM MOPS pH 7.0 (with the ionic strength adjusted to 200 mM using potassium chloride) containing various urea concentrations covering the unfolding transition of the NTD (2.2 to 4.5 M urea). Trp fluorescence was excited at 280 nm using a xenon lamp and an optical high-transmittance band-pass filter. Fluorescence emission was collected at >315 nm using an optical cutoff filter. Analyzed kinetic transients were an average of 20 individual T-jumps.

Data analysis. *PET-FCS.* Recorded ACFs, $G(\tau)$, were fitted using an analytical model for translational diffusion of a molecule that exhibits chemical relaxations.[45] The ACFs of NTD constructs fitted well to a model for diffusion of a globule with two independent, single-exponential relaxations:

$$G(\tau) = \frac{1}{N}\left(1 + \frac{\tau}{\tau_D}\right)^{-1}\left(1 + a_1\exp\left(-\frac{\tau}{\tau_1}\right) + a_2\exp\left(-\frac{\tau}{\tau_2}\right)\right) \quad (1)$$

τ is the lag time, N is the average number of molecules in the detection focus, τ_D is the diffusion time constant, a_1 and a_2 are the amplitudes of relaxations 1 and 2, and τ_1 and τ_2 are the according time constants. The application of a model for diffusion in two dimensions was of sufficient accuracy because the two horizontal dimensions (x, y) of the detection focus were much smaller than the lateral dimension (z) in the applied setup. All ACFs and data fits shown in figures were normalized to N for reasons of clarity.

Protein Folding. Equilibrium denaturation data were fitted using the thermodynamic model for a two-state equilibrium between native and denatured states. The spectroscopic signal S can be expressed as a function of denaturant concentration:[46]

$$S([\text{urea}]) = \frac{\alpha_N + \beta_N[\text{urea}] + (\alpha_D + \beta_D[\text{urea}])\exp(-\Delta G_{D-N}([\text{urea}])/RT)}{1 + \exp(-\Delta G_{D-N}([\text{urea}])/RT)} \quad (2)$$

α_N, β_N, α_D, and β_D are the linearly sloping baselines of native and denatured states, R is the gas constant, T the temperature, and ΔG_{D-N} the difference in free energy between native (N) and denatured (D) state.

ΔG_{D-N} as a function of denaturant is described by the linear-free-energy relationship:[47]

$$\Delta G_{D-N}([\text{urea}]) = \Delta G_{D-N} - m_{D-N}[\text{urea}] \quad (3)$$

m_{D-N} is the equilibrium m-value that describes the sensitivity of the folding equilibrium to denaturant.

Kinetic transients from T-jump experiments were fitted to a single-exponential function containing a linear baseline drift to account for photobleaching of Trp:

$$S(t) = a\exp(-k_{obs}t) + bt + c \quad (4)$$

$S(t)$ is the fluorescence signal as a function of time, a is the amplitude, and k_{obs} the observed rate constant of the relaxation. The parameter b describes the linear drift of the baseline. k_{obs} is the sum of the microscopic rate constants for folding and unfolding (k_f and k_u):[29]

$$k_{obs} = k_f + k_u \quad (5)$$

The change of k_{obs} as a function of denaturant concentration was analyzed by fitting the data to the chevron model for a barrier-limited two-state transition that follows the linear-free-energy relationship:[29]

$$\log k_{obs}([\text{urea}]) = \log[k_f\exp(-m_{TS-D}[\text{urea}]/RT) + k_u\exp(m_{TS-N}[\text{urea}]/RT)] \quad (6)$$

m_{TS-D} and m_{TS-N} are the kinetic m-values of folding and unfolding, respectively, where TS denotes the transition state separating denatured and native free energy wells. k_f and k_u are the microscopic rate constants of folding and unfolding, respectively, under standard conditions in the absence of denaturant.

■ ASSOCIATED CONTENT

Ⓢ Supporting Information

Steady-state Trp fluorescence spectra, additional PET-FCS data, and additional T-jump transients together with their analysis. This material is available free of charge via the Internet at http://pubs.acs.org.

■ AUTHOR INFORMATION

Corresponding Author

hannes.neuweiler@uni-wuerzburg.de

Notes

The authors declare no competing financial interest.

■ ACKNOWLEDGMENTS

The authors thank the Deutsche Forschungsgemeinschaft (DFG) for financial support (Grant # NE 1201/3-1).

■ REFERENCES

(1) Vollrath, F.; Knight, D. P. *Nature* **2001**, *410*, 541.
(2) Heim, M.; Keerl, D.; Scheibel, T. *Angew. Chem., Int. Ed.* **2009**, *48*, 3584.
(3) Hinman, M. B.; Jones, J. A.; Lewis, R. V. *Trends Biotechnol* **2000**, *18*, 374.
(4) Eisoldt, L.; Thamm, C.; Scheibel, T. *Biopolymers* **2011**, *97*, 355.
(5) Askarieh, G.; Hedhammar, M.; Nordling, K.; Saenz, A.; Casals, C.; Rising, A.; Johansson, J.; Knight, S. D. *Nature* **2010**, *465*, 236.
(6) Vollrath, F.; Knight, D. P.; Hu, X. W. *Proc. R. Soc. London, Ser. B* **1998**, *265*, 817.
(7) Gaines, W. A.; Sehorn, M. G.; Marcotte, W. R., Jr. *J. Biol. Chem.* **2010**, *285*, 40745.
(8) Hagn, F.; Thamm, C.; Scheibel, T.; Kessler, H. *Angew. Chem., Int. Ed.* **2011**, *50*, 310.
(9) Landreh, M.; Askarieh, G.; Nordling, K.; Hedhammar, M.; Rising, A.; Casals, C.; Astorga-Wells, J.; Alvelius, G.; Knight, S. D.; Johansson, J.; Jornvall, H.; Bergman, T. *J. Mol. Biol.* **2010**, *404*, 328.
(10) Schwarze, S.; Zwettler, F. U.; Johnson, C. M.; Neuweiler, H. *Nat. Commun.* **2013**, *4*, 2815.
(11) Jaudzems, K.; Askarieh, G.; Landreh, M.; Nordling, K.; Hedhammar, M.; Jornvall, H.; Rising, A.; Knight, S. D.; Johansson, J. *J. Mol. Biol.* **2012**, *422*, 477.
(12) Kronqvist, N.; Otikovs, M.; Chmyrov, V.; Chen, G.; Andersson, M.; Nordling, K.; Landreh, M.; Sarr, M.; Jornvall, H.; Wennmalm, S.; Widengren, J.; Meng, Q.; Rising, A.; Otzen, D.; Knight, S. D.; Jaudzems, K.; Johansson, J. *Nat. Commun.* **2014**, *5*, 3254.
(13) Weiss, S. *Nat. Struct. Biol.* **2000**, *7*, 724.
(14) Joo, C.; Balci, H.; Ishitsuka, Y.; Buranachai, C.; Ha, T. *Annu. Rev. Biochem.* **2008**, *77*, 51.
(15) Schuler, B.; Eaton, W. A. *Curr. Opin. Struct. Biol.* **2008**, *18*, 16.
(16) Henzler-Wildman, K.; Kern, D. *Nature* **2007**, *450*, 964.
(17) Schuler, B.; Hofmann, H. *Curr. Opin. Struct. Biol.* **2013**, *23*, 36.
(18) Doose, S.; Neuweiler, H.; Sauer, M. *ChemPhysChem* **2009**, *10*, 1389.
(19) Neuweiler, H.; Johnson, C. M.; Fersht, A. R. *Proc. Natl. Acad. Sci. U. S. A.* **2009**, *106*, 18569.
(20) Sauer, M.; Neuweiler, H. *Methods Mol. Biol.* **2014**, *1076*, 597.
(21) Vaiana, A. C.; Neuweiler, H.; Schulz, A.; Wolfrum, J.; Sauer, M.; Smith, J. C. *J. Am. Chem. Soc.* **2003**, *125*, 14564.
(22) Haustein, E.; Schwille, P. *Annu. Rev. Biophys. Biomol. Struct.* **2007**, *36*, 151.
(23) Zhu, R.; Li, X.; Zhao, X. S.; Yu, A. *J. Phys. Chem. B* **2011**, *115*, 5001.
(24) Doose, S.; Neuweiler, H.; Barsch, H.; Sauer, M. *Proc. Natl. Acad. Sci. U. S. A.* **2007**, *104*, 17400.
(25) Daidone, I.; Neuweiler, H.; Doose, S.; Sauer, M.; Smith, J. C. *PLoS Comput. Biol.* **2010**, *6*, e1000645.
(26) Kubelka, J.; Hofrichter, J.; Eaton, W. A. *Curr. Opin. Struct. Biol.* **2004**, *14*, 76.
(27) Lange, O. F.; Lakomek, N. A.; Fares, C.; Schroder, G. F.; Walter, K. F.; Becker, S.; Meiler, J.; Grubmüller, H.; Griesinger, C.; de Groot, B. L. *Science* **2008**, *320*, 1471.
(28) Bourgeois, D.; Vallone, B.; Schotte, F.; Arcovito, A.; Miele, A. E.; Sciara, G.; Wulff, M.; Anfinrud, P.; Brunori, M. *Proc. Natl. Acad. Sci. U. S. A.* **2003**, *100*, 8704.
(29) Jackson, S. E.; Fersht, A. R. *Biochemistry* **1991**, *30*, 10428.
(30) Wallace, J. A.; Shen, J. K. *J. Phys. Chem. Lett.* **2012**, *3*, 658.
(31) Andersson, M.; Chen, G.; Otikovs, M.; Landreh, M.; Nordling, K.; Kronqvist, N.; Westermark, P.; Jornvall, H.; Knight, S.; Ridderstrale, Y.; Holm, L.; Meng, Q.; Jaudzems, K.; Chesler, M.; Johansson, J.; Rising, A. *PLoS Biol.* **2014**, *12*, e1001921.
(32) Frauenfelder, H.; Sligar, S. G.; Wolynes, P. G. *Science* **1991**, *254*, 1598.
(33) Bryngelson, J. D.; Onuchic, J. N.; Socci, N. D.; Wolynes, P. G. *Proteins* **1995**, *21*, 167.
(34) Baldwin, A. J.; Kay, L. E. *Nat. Chem. Biol.* **2009**, *5*, 808.
(35) Neuweiler, H.; Banachewicz, W.; Fersht, A. R. *Proc. Natl. Acad. Sci. U. S. A.* **2010**, *107*, 22106.
(36) Teufel, D. P.; Johnson, C. M.; Lum, J. K.; Neuweiler, H. *J. Mol. Biol.* **2011**, *409*, 250.
(37) Boehr, D. D.; Nussinov, R.; Wright, P. E. *Nat. Chem. Biol.* **2009**, *5*, 789.
(38) Breslauer, D. N.; Lee, L. P.; Müller, S. J. *Biomacromolecules* **2009**, *10*, 49.
(39) Ortlepp, C. S.; Gosline, J. M. *Biomacromolecules* **2004**, *5*, 727.
(40) Knight, D. P.; Vollrath, F. *Naturwissenschaften* **2001**, *88*, 179.
(41) Jackson, S. E. *Folding Des.* **1998**, *3*, R81.
(42) Myers, J. K.; Oas, T. G. *Annu. Rev. Biochem.* **2002**, *71*, 783.
(43) Gelman, H.; Gruebele, M. *Q. Rev. Biophys.* **2014**, *47*, 95.
(44) Pace, C. N.; Grimsley, G. R.; Scholtz, J. M. *J. Biol. Chem.* **2009**, *284*, 13285.
(45) Krichevsky, O.; Bonnet, G. *Rep. Prog. Phys.* **2002**, *65*, 251.
(46) Santoro, M. M.; Bolen, D. W. *Biochemistry* **1988**, *27*, 8063.
(47) Tanford, C. *Adv. Protein Chem.* **1968**, *23*, 121.